Environmental Science & Technology

pubs.acs.org/est

Article

Ionic Strength-Dependent Attachment of *Pseudomonas aeruginosa* PAO1 on Graphene Oxide Surfaces

Xinxin Jing, Yichao Wu,* Dengjun Wang, Chenchen Qu, Jun Liu, Chunhui Gao, Abdelkader Mohamed, Qiaoyun Huang, Peng Cai,* and Noha Mohamed Ashry

Cite This: *Environ. Sci. Technol.* 2022, 56, 16707−16715

Read Online

ACCESS | Metrics & More | Article Recommendations | Supporting Information

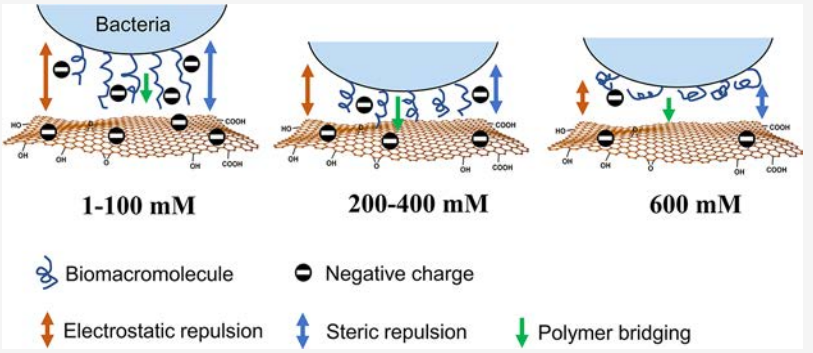

ABSTRACT: Graphene oxide (GO) is a widely used antimicrobial and antibiofouling material in surface modification. Although the antibacterial mechanisms of GO have been thoroughly elucidated, the dynamics of bacterial attachment on GO surfaces under environmentally relevant conditions remain largely unknown. In this study, quartz crystal microbalance with dissipation monitoring (QCM-D) was used to examine the dynamic attachment processes of a model organism *Pseudomonas aeruginosa* PAO1 onto GO surface under different ionic strengths (1−600 mM NaCl). Our results show the highest bacterial attachment at moderate ionic strengths (200−400 mM). The quantitative model of QCM-D reveals that the enhanced bacterial attachment is attributed to the higher contact area between bacterial cells and GO surface. The extended Derjaguin−Landau−Verwey−Overbeek (XDLVO) theory and atomic force microscopy (AFM) analysis were employed to reveal the mechanisms of the bacteria−GO interactions under different ionic strengths. The strong electrostatic and steric repulsion at low ionic strengths (1−100 mM) was found to hinder the bacteria−GO interaction, while the limited polymer bridging caused by the collapse of biopolymer layers reduced cell attachment at a high ionic strength (600 mM). These findings advance our understanding of the ionic strength-dependent bacteria−GO interaction and provide implications to further improve the antibiofouling performance of GO-modified surfaces.

KEYWORDS: *biofouling, graphene oxide, ionic strength, bacterial adhesion, electrostatic repulsion, steric interaction*

INTRODUCTION

Graphene oxide (GO), the oxygen-functionalized graphene, is one of the most promising graphene-based materials in large-scale production and commercialization.[1−3] Owing to the unique properties, including two-dimensional nature, electrical conductivity, mechanical strength, and antimicrobial activity, GO and its chemically modified derivatives hold great prospects in a myriad of applications ranging from water purification to biomedical engineering.[4−7] The surfaces modified with GO exhibit enhanced antibacterial properties and inhibitory effects on biofilm formation via direct physical damages and reactive oxygen species (ROS)-mediated oxidative stress, thus improving antibiofouling and biocidal performance.[8−10]

Although the antibacterial activities of GO have been largely elucidated, the attachment of bacteria onto GO surface remains contentious. The direct contact between bacterial cells and GO is a prerequisite for GO's antibacterial activities. Nonetheless, enhanced bacterial attachment compromises the bactericidal efficacy and causes severe fouling. Previous atomic force microscopy (AFM)-based studies revealed that the bacteria−GO interaction was predominantly repulsive due to the electrostatic and steric repulsion between deprotonated carboxylate groups in GO and the negatively charged cell surface.[11,12] On the other hand, the enhanced bacterial attachment to GO-coated organic and inorganic surfaces via

Received: December 19, 2021
Revised: October 30, 2022
Accepted: November 1, 2022
Published: November 15, 2022

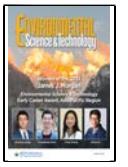

hydrophobic interaction has been demonstrated.[13−15] These contradictory conclusions are mainly derived from the various parameters influencing the interfacial behaviors. It has been recognized that the chemical properties of the background electrolyte such as ionic strength govern the extent and mechanisms of bacterial attachment to surfaces.[16−18] Moreover, the lack of real-time and quantitative analysis of the bacterial deposition dynamics on GO surface also leads to divergent results from different investigators.[12,19,20] As bacterial attachment onto GO is critical in determining GO's antibiofouling and antibacterial performance, it is crucial to reveal the effect of solution chemistry on the dynamic bacterial attachment processes on GO surface and develop a comprehensive understanding of bacteria−GO interaction.

In this study, we aim to unravel the effect of ionic strength on the dynamic attachment of a model biofouling bacterium, *Pseudomonas aeruginosa* PAO1, on the GO surface. *P. aeruginosa* PAO1 is ubiquitous in a wide variety of environments, which have been found to be prevalent in water treatment systems and clinical settings.[21−24] Quartz crystal microbalance with dissipation monitoring (QCM-D) and confocal laser scanning microscopy (CLSM) were used to monitor the dynamic attachment process. The bacterial adhesion behavior on the GO surface was interpreted by extended Derjaguin−Landau−Verwey−Overbeek (XDLVO) theory. Atomic force microscopy (AFM) analysis was further used to investigate the adhesion force of bacteria onto the GO surface, as well as the role of surface biopolymers. Taken together, this study provides a fundamental understanding of the bacterial attachment onto the GO surface under different ionic strengths.

MATERIALS AND METHODS

Preparation and Characterization of GO. The GO powder (purity > 99.5 wt %) was purchased from Time nano Chengdu Organic Chemicals Co. Ltd. The thickness and the lateral size of GO nanosheets are 0.55−1.2 nm and 0.5−3 μm, respectively. GO suspension (0.5 mg mL^{-1}) was prepared and dispersed in methanol by ultrasonic treatment in a water bath for 30 min. The detailed characterization of GO is shown in Figures S1−S4.

Bacteria and Culture Condition. *P. aeruginosa* PAO1 and the Δ*pel*-Δ*psl* mutant were provided by Prof. Liang Yang (Southern University of Science and Technology, China). Strains were maintained as glycerol stocks (LB broth containing 20% (v/v) glycerol) at −80 °C. Briefly, cultures were grown in LB broth with shaking at 200 rpm. After cultivation at 30 °C overnight, the cells were collected at the stationary phase, washed three times with 0.9% NaCl solution, and then resuspended in the different electrolyte solutions (1, 45, 100, 200, 400, and 600 mM NaCl) to a final optical density (OD_{600}) of 0.2. The NaCl solutions have been sterilized by autoclaving before use. An OD_{600} of 0.2 corresponded to 2.53 ± 0.46 × 10^8 cells mL^{-1}. The pH of cell suspension was adjusted to 7.0 using a dilute NaOH or HCl solution. All of the operations were carried out under sterile conditions in the laminar flow cabinet. After 12 h incubation in the electrolytes with different ionic strengths, the bacterial viability was assessed via the Live/Dead BacLight viability kit. The bacterial EPS was extracted using the cation-exchange resin method and then quantified via colorimetric methods.[25,26] The ionic strengths had a negligible influence on the cell viability and EPS content (Figure S5 and Table S1).

QCM-D Measurements. QCM-D system (Q-Sense, Gothenburg, Sweden) was used to investigate the bacterial attachment kinetics on sensors by recording dissipation values and the frequency shift (3rd, 5th, 7th, and 9th harmonics).[27] Specifically, the AT-cut 5 MHz gold-coated quartz crystals (QSX301, Q-sense, Sweden) were used in this experiment. A solution composed of 30% hydrogen peroxide, ammonia, and deionized water (1:1:5 ratio) was used to clean the sensors at 75 °C for 5 min. Afterward, the sensors were rinsed with ultrapure water and dried under a nitrogen gas stream. The gold-plated sensors were spin-coated with GO (0.5 mg mL^{-1}) at 6000 rpm to obtain a thin layer.[28,29] The GO-coated sensor was examined by SEM and AFM to confirm that GO was uniformly covered on the surface (Figures S6 and S7). The sterile NaCl solution without bacteria was introduced into the QCM-D chamber until the baseline was stabilized for at least 4 h. To monitor bacterial attachment under a well-defined and constant condition, the bacterial suspension was then continuously fed with a flow rate of 100 μL min^{-1}. At four different overtones (n = 3, 5, 7, and 9), the shifts of frequency (Δf, Hz) and energy dissipation (ΔD) were monitored for 10 h.

Raman Spectroscopy. Raman spectra were acquired from a confocal Raman microscopy equipped with a 600 g mm^{-1} grating and a 532 nm laser (Horiba LabRAM HR 800). Raman mapping was performed to confirm the completeness of GO coating on QCM-D sensors. For each Raman mapping measurement, 497 spectra were collected within an elliptical area of 40 μm × 50 μm. The acquisition time for each spectrum was 8 s. The Raman mapping images at 1600 cm^{-1} demonstrated that the gold-plated sensors were completely covered by GO before and after QCM-D experiments (Figure S8).

Modeling of QCM-D Data. QCM-D quantitative model was used to further analyze the mechanical properties of *P. aeruginosa* PAO1 attachment on the GO surface,[30] including the bacterial contact elasticity (κ_c), contact damping (ξ_c), density of adhering bacteria (N_p), and contact region (r_c). The bacterial cells were approximated as spherical particles with a radius of 1 μm and a mass of 1.348 g cm^{-3}.[30]

When bacteria adhere to the sensor, the QCM-D signal is interpreted according to eqs 1 to 3, which bind the complex shifts Δf^* in the resonance frequency Δf_n and dissipation $\Delta\Gamma_n$. The shifts Δf_* are related to complex load impedance ΔZ_L^*, which includes imaginary and real parts as follows

$$\Delta f^* = \Delta f + i\Delta\Gamma \tag{1}$$

$$\Delta f_n = -\frac{f_F}{\pi Z_q}\mathrm{Im}(\Delta Z_L^*) \tag{2}$$

$$\Delta\Gamma_n = \frac{f_F n}{2}\Delta D_n = \frac{f_F}{\pi Z_q}\mathrm{Re}(\Delta Z_L^*) \tag{3}$$

where f_F and Z_q are the fundamental frequency (5 MHz) and load impedance (8.8 × 10^6 kg m^{-2} s^{-1}) of the quartz crystal, respectively; n is the overtone number; and $\mathrm{Im}(\Delta Z_L^*)$ and $\mathrm{Re}(\Delta Z_L^*)$ represent the imaginary and real parts of ΔZ_L^*, respectively.

According to the equivalent circuit, the total Δf_{total}^* is determined by parallel connected loads of oscillating particle and contact region

https://doi.org/10.1021/acs.est.1c08672
Environ. Sci. Technol. 2022, 56, 16707−16715

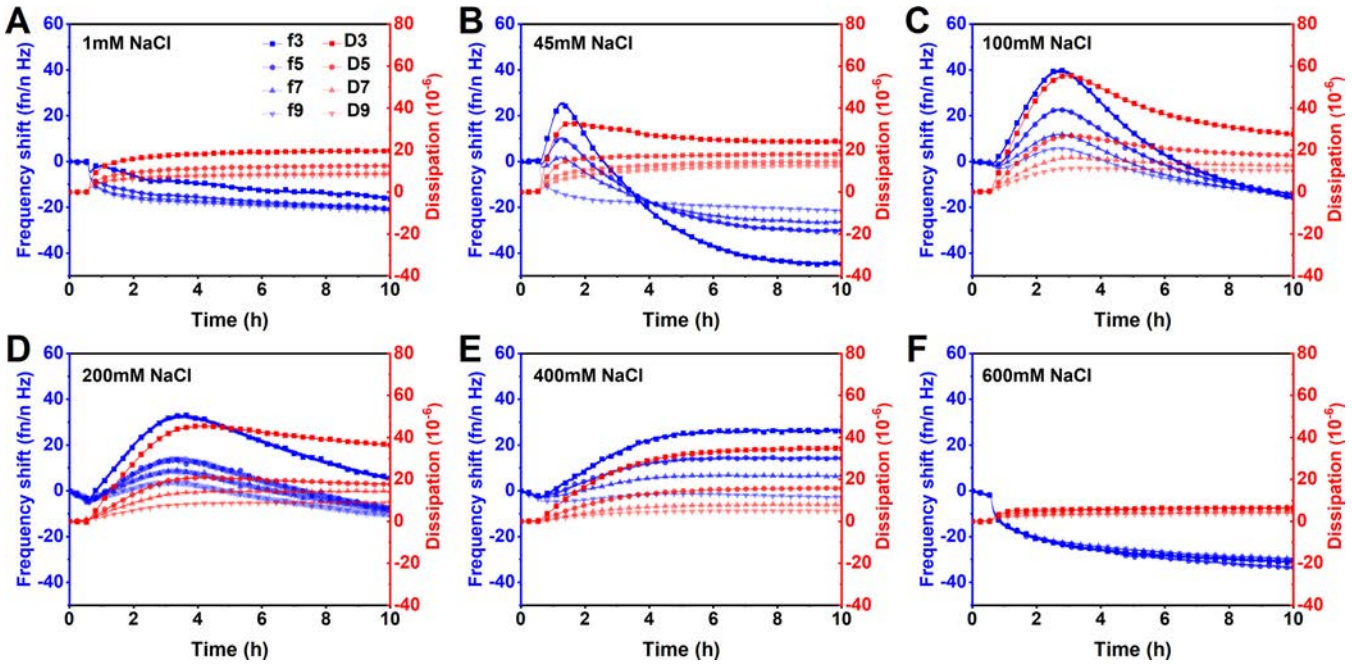

Figure 1. QCM-D frequency and dissipation shifts versus time for *P. aeruginosa* PAO1 attachment process at the ionic strengths of 1 mM (A), 45 mM (B), 100 mM (C), 200 mM (D), 400 mM (E), and 600 mM (F). Frequency shift and dissipation shift using QCM-D data for 3rd, 5th, 7th, and 9th overtones.

$$\Delta f^*_{\text{total}} = \left(\frac{1}{\Delta f^*_{\text{p}}} + \frac{1}{\Delta f^*_{\text{c}}} \right)^{-1} \tag{4}$$

where Δf^*_{p} and Δf^*_{c} are the impedance of free oscillating bacteria loads and contact region, respectively (see the Supporting Information for details).

To obtain the best data fit, the minimized deviation (d) between the recorded data of QCM-D (Δf_i^{exp} and $\Delta \Gamma_i^{\text{exp}}$) and the model-predicted values ($\Delta f_i^{\text{model}}$ and $\Delta \Gamma_i^{\text{model}}$) is calculated as follows

$$d = \sqrt{\sum_i (\Delta f_i^{\text{exp}} - \Delta f_i^{\text{model}})^2} + \sqrt{\sum_i (\Delta \Gamma_i^{\text{exp}} - \Delta \Gamma_i^{\text{model}})^2} \tag{5}$$

where 95% confidence intervals were constructed by Monte Carlo simulation.[31]

Confocal Laser Scanning Microscopy (CLSM) Measurement. During bacterial attachment processes, the sensors were collected and observed by CLSM (Fluoview FV-1000, Olympus, Germany) to evaluate the number of cells attached on the GO surface. The bacteria on the GO-coated sensor were stained using SYTO 9 and detected by excitation at 488 nm and emission at 500 nm. Seven images were taken for each ionic strength condition, and the number of cells was estimated using IMARIS software.[32]

AFM Analysis. The adhesion force between bacteria and GO was measured using a triangular-shaped standard AFM cantilever (MLCT-O10, Bruker), which was modified with 10-μm-radius silica beads (Bangs Laboratories). The silica beads were cleaned with ultrapure water and then attached to triangular-shaped tipless cantilevers by UV-curable glue (Adhesive 63, Norland Products) using an AFM micromanipulator.[33] The AFM cantilevers with silica beads were exposed to ultraviolet light for 30 min and then washed with ultrapure water. The washed AFM probe was successively immersed in a poly-L-lysine (PLL) solution (0.01%) and a bacterial suspension (OD_{600} = 1.0) for 1 min each to immobilize bacterial cells on the PLL functionalized AFM cantilevers.[34] The GO-coated substratum was prepared by dropping the GO suspension onto the glass sheet and then dried in an oven at 120 °C. The GO coating was characterized by SEM and AFM to ensure that the substratum was completely covered by GO (Figures S6 and S7). A MultiMode 8 AFM system with a NanoScope V controller (Bruker) was employed to obtain the force curves of bacteria. The NaCl solutions with different ionic strengths were adjusted to a pH of 7.0 using dilute NaOH or HCl solutions and then injected into the AFM fluid cell. All force curves were determined in the contact mode in NaCl solutions. The force curves were carried out at a scan rate of 1 Hz. The ramp size and trigger threshold were set to 1 μm and 2 nN, respectively. The contact time was 0 s. The adhesive energy (E_{adh}) was calculated by integrating the area below the x-axis and above the retraction curves.[35]

Extended Derjaguin–Landau–Verwey–Overbeek (XDLVO) Analysis. The extended DLVO theory was used to describe the cell–GO interaction at various ionic strengths (see the Supporting Information for details). The total XDLVO interaction energy (W^{XDLVO}) is the sum of the Lifshitz–van der Waals, electrostatic, and Lewis acid–base interaction energies. The zeta potentials of GO and bacterial cells at different ionic strengths were measured at pH = 7 using a Zetasizer analyzer (Nano ZEN 3600, Malvern, U.K.). The contact angle of GO and bacterial cells was measured by the sessile drop technique using a Drop Shape Analyzer DSA100 (Krüss GmbH, Germany).[36] Water, formamide, and diiodomethane were used as probe liquids to determine surface tension components. The surface tension components for *P. aeruginosa* PAO1 and GO are summarized in Table S2.

https://doi.org/10.1021/acs.est.1c08672
Environ. Sci. Technol. 2022, 56, 16707–16715

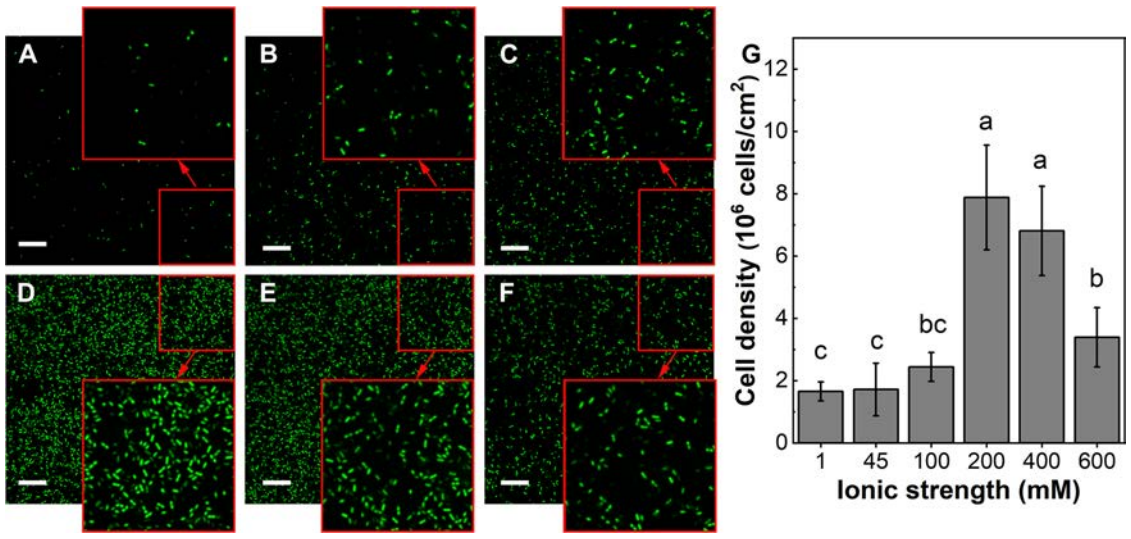

Figure 2. CLSM images of *P. aeruginosa* PAO1 after 9.5 h of cell attachment on GO surface at 1 mM (A), 45 mM (B), 100 mM (C), 200 mM (D), 400 mM (E), and 600 mM (F). Surface cell density is calculated by CLSM imaging analyses (G). The scale bar is 20 μm. The different letters above each column represent statistical significance ($P < 0.05$, ANOVA).

Steric Interaction Analysis. XDLVO and steric models were employed to explain the AFM force measurements. The difference between AFM approaching force and the predicted XDLVO force was fitted to the steric model. According to the previous report by Butt et al.,[37] the interaction force (F_{st}) is associated with the force per unit area of the AFM tip surface, which is given as follows

$$F_{st} = 50 k_B T a L_0 \Gamma^{3/2} e^{-(2\pi h/L_0)} \quad (6)$$

where k_B is the Boltzmann constant (1.38×10^{-23} J K^{-1}), T is the temperature (298 K), L_0 is the thickness of the bacterial surface biopolymer brush (nm), a is the radius of the silica bead,[38] Γ is the grafting density of the biopolymer layer, and h is the distance between the AFM tip and the GO surface. For each ionic strength, more than 35 approaching curves were collected to fit the steric model.

The steric interaction energy (W^{steric}) between the bacterial surface and GO surface can be obtained as follows[39,40]

$$W^{steric} = \frac{8\pi k_B T {L_0}^2 R}{35 S^3}\left[28\left(\frac{L_0}{d}\right)^{1/4} - \frac{20}{11}\left(\frac{d}{L_0}\right)^{11/4} + 12\left(\frac{d}{L_0}\right) - \frac{420}{11}\right] \quad (7)$$

where R is the radius of bacteria (0.5 μm) and S is the mean distance between anchoring sites on the cell surface (nm) that can be calculated by grafting density (Γ) according to the following equation[40]

$$S \approx \frac{1}{\Gamma^2} \quad (8)$$

Statistics Analysis. Statistical significance analysis was performed using the Student's t test, and $P < 0.05$ indicates a significant difference within the 95% confidence interval.

RESULTS

Dynamics of Cell Attachment on GO Surface. QCM-D was used to assay the cell attachment dynamics onto the GO surface under different ionic strengths. After the injection of bacterial cells, dissipation (ΔD) increases during the cell attachment phase, while frequency shift (Δf) differs as a function of ionic strength, especially at the third overtone (Δf_3) (Figures 1 and S9). A two-stage attachment is observed based on Δf_3 at the ionic strengths of 45−200 mM. In the first stage, the Δf_3 values increase and reach the peak (Figure 1). The positive Δf is caused by the oscillation of a soft and thick bacterial layer on the GO surface, which counterbalances the added inertia.[41,42] The significantly increased Δf and ΔD indicate the substantial bacterial attachment at moderate ionic strengths (200−400 mM). The duration of the soft bacterial layer is prolonged with the increase of ionic strength from 45 to 400 mM. In the second stage, the frequency decreases to a negative value (Figure 1), suggesting the transition of the attached bacterial layer from soft to rigid. Different from the moderate ionic strengths (45−400 mM), the Δf values decrease upon the cell attachment at the ionic strength of 1 and 600 mM, which indicates the development of a rigid bacterial layer on the GO surface.

The cell densities on QCM-D sensors were analyzed by microscopic observation (Figures 2 and S10). Upon the introduction of bacterial cells, a rapid bacterial attachment was observed for the moderate ionic strengths (45−400 mM) (Figure S10). The surface cell densities then decreased and gradually approached certain values. The dynamics of surface cell densities at moderate ionic strengths (45−400 mM) are consistent with the observed changes in Δf, which shows an initial increase followed by a gradual decrease (Figures 1 and S10). After 10 h bacterial attachment, the surface cell densities are higher with increasing ionic strengths (from 1 to 400 mM) and reach a maximum at the ionic strength of 200 and 400 mM. Remarkably, the surface cell density at the ionic strength of 600 mM is significantly lower than those at 200 and 400 mM. Therefore, the QCM-D measurements reveal a non-monotonic effect of ionic strength on bacterial attachment to the GO surface.

Mechanical Properties of the Attached Bacteria. To further characterize the interaction between bacteria and the GO surface, the recorded data (Δf and ΔD) at 10 h were fitted

https://doi.org/10.1021/acs.est.1c08672
Environ. Sci. Technol. 2022, 56, 16707−16715

to the quantitative model of QCM-D. The linear dependence between Δf and the overtone number (Figure S11A−F) and the deviation of observed Δf values from the freely oscillating sphere model prediction (solid line in Figure S11) indicate the importance of contact elasticity in bacterial attachment, especially at the ionic strengths of 200 and 400 mM. The bandwidth shift ($\Delta\Gamma$) is correlated with $n^{(1/2)}$ at the ionic strengths of 1−100 and 600 mM (Figure S11G−I,L), suggestive of a viscous dissipation (Figure S12). These results can be further demonstrated by contact elasticity (κ_c) and contact damping (ξ_c). The bacterial attachment at ionic strengths of 200 and 400 mM demonstrates the highest κ_c and contact radius (r_c). Since κ_c is mainly determined by the work of adhesion between bacteria and GO surfaces,[30] the highest κ_c and r_c values at 200 and 400 mM suggest a strong bacteria−GO interaction at the moderate ionic strength. The observed cell densities are positively correlated with r_c ($P < 0.05$) (Figure 3), indicating a higher contact radius contributing to more cell adhesion. Although the surface cell densities calculated from the model fitting are lower than the CLSM result (Table 1), the trend of predicted surface cell densities (N_p) is consistent with the microscope data (Figures 2 and S13). This discrepancy in surface cell densities was observed in previous studies, which demonstrated that QCM-D only senses strongly attached cells on sensor surfaces.[30,43,44] It indicates that a large fraction of attached cells observed by microscopy loosely contacted with the GO surface.

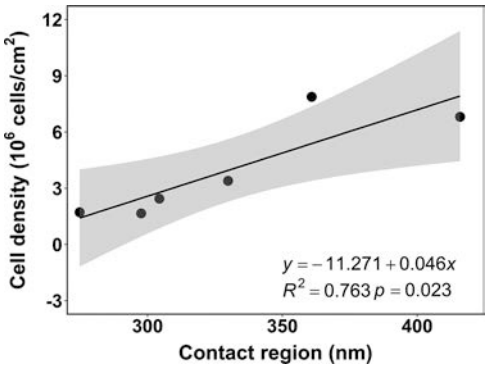

Figure 3. Linear correlation between surface cell densities and contact region at different ionic strengths. The gray shaded area denotes the 95% confidence interval.

Effect of Ionic Strength on Adhesion and Biopolymer Conformation. AFM analysis was performed to reveal the adhesive energy between bacteria and GO surfaces. The peak adhesion force (F_{peak}) during retraction of *P. aeruginosa* PAO1 away from the GO surface increases significantly with increasing ionic strength from 1 to 200 mM and remains constant when the ionic strengths are higher than 200 mM (Figures 4A and S14−S16). The rupture distance (L_R) in the retraction process significantly increases with the increase in ionic strength, approaching a maximum (569.23 ± 190.44 nm) at 100 mM (Figures 4B and S16), and decreases when the ionic strength is higher than 100 mM. Compared with those at moderate ionic strengths, the reduced rupture distance contributes to a significantly lower adhesive energy at 600 mM (Figure 4C), which is consistent with the reduced surface cell density.

The long rupture distance and sawtooth-shaped force curves implicate the critical role of surface biopolymers in bacterial adhesion. The difference between AFM approaching force and the predicted XDLVO force was fitted to the steric model to elucidate the role of ionic strength on biopolymer conformation. The average thickness of the extended bacterial cell-surface biomolecules decreases with the increase of ionic strength (Figure 4D), while the grafting density exhibits an opposite trend (Figure 4E). The ionic strength-dependent changes in the brush thickness and grafting density are absent for the polysaccharide-deficient mutant strain (Δ*pel*-Δ*psl*) (Figure S17), which highlighted the contribution of surface biopolymers in steric interaction. The collapsed biopolymer layer on the cell surface, caused by the electrostatic stabilization and hydration effect,[45−49] reduces the binding sites for polymer bridging and results in a shorter rupture distance at the ionic strength of 600 mM (Figure 4B). Moreover, the extended brush layer at 1−100 mM NaCl also corresponds to short rupture distances (Figure 4B), suggesting that the polymer bridging at low ionic strengths is prevented by the strong electrostatic repulsion (Figure S18).

Interaction Energy between *P. aeruginosa* PAO1 and GO. As the presence of bacterial biopolymer causes steric hindrance between bacteria and GO surface, the combined influence of steric repulsion and XDLVO interactions on bacterial attachment was investigated (Figure 5). The negatively charged bacterial cells and GO give rise to a repulsive electrostatic energy barrier, which reduces with increasing ionic strength due to compression of the electrostatic double layer (Figures S18 and S19). Meanwhile, the repulsive hydration effects exhibit an opposite trend, showing increased hydration repulsion at high ionic strength (Figure S18). With the same van der Waals attraction at different ionic strengths, the XDLVO interactions at 1−45 mM are mainly repulsive (Figure 5A). The steric repulsion is monotonically decreased with increasing ionic strength owing to the collapsed biopolymer layer at a high ionic strength (Figure 5B). Consequently, the total interaction energy profile based on XDLVO and steric interactions shows the existence of the

Table 1. Fitted Parameters for *P. aeruginosa* PAO1 Attachment on Graphene Oxide Surface at Different Ionic Strengths[a]

	fitted parameters				
ionic strength (mM)	κ_c(N m^{-1})	ξ_c(10^{-8} Pa·m·s)	N_p(10^5 cm^{-2})	r_c (nm)	d[b]
1	7.03 (7.01, 7.04)	119.84 (113.66, 128.13)	1.05 (1.00, 1.09)	297.63 (297.33, 297.85)	175.51
45	5.53 (5.52, 5.55)	92.24 (88.54, 95.65)	1.75 (1.71, 1.80)	274.86 (274.67, 275.05)	130.20
100	7.52 (7.43, 7.60)	58.83 (55.37, 62.44)	1.87 (1.79, 1.96)	304.36 (303.25, 305.44)	160.00
200	12.52 (7.48, 17.39)	27.41 (21.74, 31.75)	3.16 (2.61, 4.13)	360.85 (303.82, 402.60)	172.63
400	19.17 (18.52, 19.88)	18.56 (17.9, 19.13)	2.91 (2.91, 2.91)	415.83 (411.11, 420.89)	106.39
600	9.56 (9.56, 9.56)	468.91 (442.69, 495.86)	0.78 (0.76, 0.79)	329.84 (329.81, 329.86)	58.03

[a]95% confidence region of parameters is given in parentheses. [b]d, deviation between experimental data and predicted values.

https://doi.org/10.1021/acs.est.1c08672
Environ. Sci. Technol. 2022, 56, 16707−16715

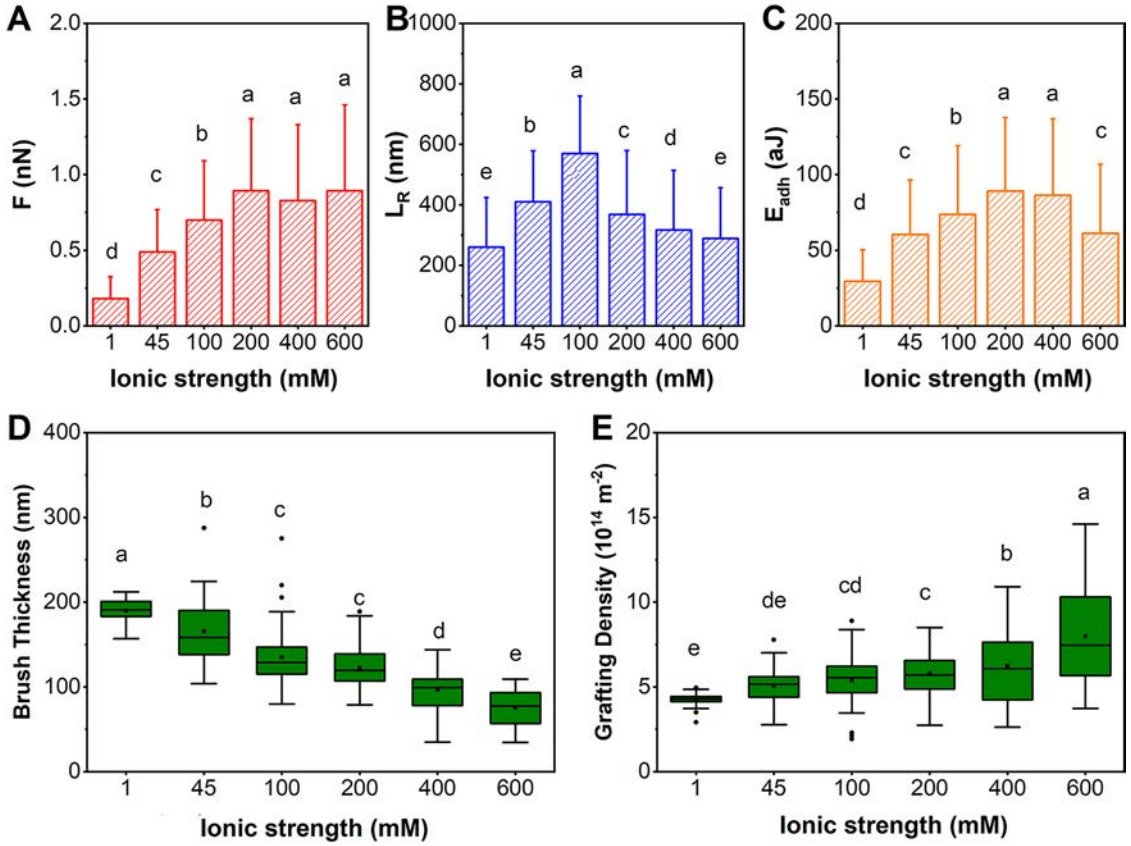

Figure 4. Average peak adhesion force (A) of *P. aeruginosa* PAO1 cells on the GO surface. Mean rupture separation (B) at which adhesion forces vanish. The average adhesive energy between bacteria and GO surfaces (C). Box plots of polymer thickness (D) and grafting density (E) for *P. aeruginosa* PAO1. Small squares and dots indicate the average values and outliers in the data. The different letters above each column represent statistical significance ($P < 0.05$, ANOVA).

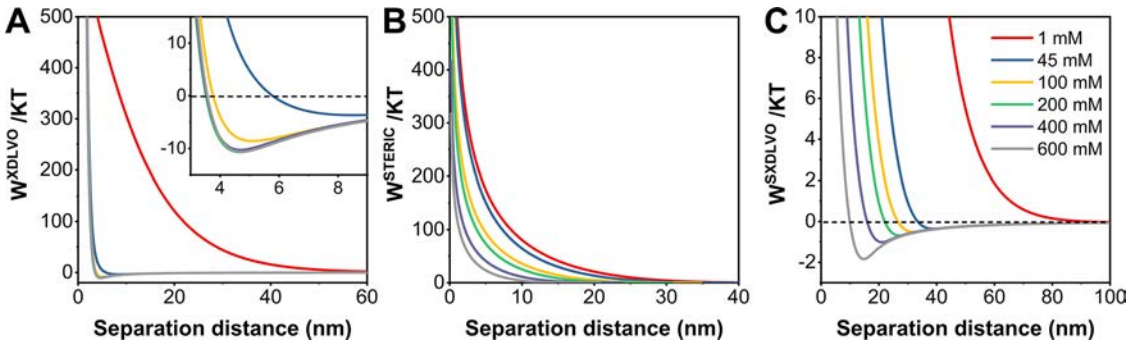

Figure 5. XDLVO energy (A), steric energy (B), and total interaction energy (C) between bacteria and GO surface as a function of separation distance at different ionic strengths.

primary minimum at the ionic strengths of 45−600 mM (Figure 5C). The reduced electrostatic and steric repulsion increases the depth of the primary minimum at high ionic strength.

The repulsive energy barrier and shallow primary minimum at the ionic strength of 1−100 mM prevent bacterial cells from attaching to GO surface, which agrees well with the observed reduced cell density (Figure 2). Meanwhile, the deep primary minimum at 600 mM does not result in an enhanced bacterial attachment. The discrepancy is likely to be attributed to the lower adhesive energy, leading to the weak and unstable bacterial adhesion on the GO surface. Therefore, the strong electrostatic and steric repulsions prevent bacterial cells from contacting the GO surface at a low ionic strength, while the weak adhesive energy induces reversible attachment and easy detachment at a high ionic strength.

DISCUSSION

GO-enabled surface modification is one promising strategy to combat the biofouling problem. Our results show that the attachment process of *P. aeruginosa* PAO1 on the GO-coated surface is significantly influenced by the ionic strength of the background electrolyte. The cell density increases with the rise of ionic strength from 1 to 400 mM. But an unexpected decrease in the surface cell density is observed at the ionic strength of 600 mM, whose ionic strength is equivalent to seawater (Figure 2). The enhanced bacterial attachment with

https://doi.org/10.1021/acs.est.1c08672
Environ. Sci. Technol. 2022, 56, 16707−16715

increased salt concentration at low ionic strengths (1−200 mM) has been demonstrated in previous studies.[18,50,51] Increasing ionic strength was found to lower the energy barrier and deepen the primary energy minimum via reducing electrostatic and steric repulsion.[52−54] Moreover, our AFM analyses reveal the adhesive energy between bacteria and GO surfaces increases with ionic strength from 1 to 400 mM. The strong adhesive energy strengthens the initial bacteria−GO interaction to yield irreversible attachment.

Further analyses reveal that the reduced cell attachment at 600 mM is attributed to the lower adhesive energy. Previous studies reported that polymer bridging can occur between the hydrophobic biomolecules such as proteinaceous adhesins of the bacteria and hydrophobic graphemic basal planes in GO.[13,55,56] The thickness of the bacterial surface biopolymer brush is found to decrease with increasing ionic strength (Figure 4D). The ionic strength-induced conformational change limits the polymer bridging between the bacteria and the GO surface, which results in the decrease of the bacterial adhesion capacity with low contact elasticity (k_c) and contact radius (r_c) at a high ionic strength (Table 1). This result is consistent with the findings of previous study that the biomolecules conformation was significantly decreased at a high ionic strength.[17,49,57]

Overall, the bacterial attachment on the GO surface is mediated by the XDLVO and steric interactions, both of which are highly dependent on ionic strength. Different strategies can be adopted to enhance antibiofouling performance in different application scenarios. In environments with ionic strengths below 45 mM or above 600 mM, the bacteria−GO interaction is featured by a weak adhesive bond. Physical cleanings such as backwashing and flushing can be employed to remove the attached cells. Meanwhile, the deep primary attractive well and strong adhesive energy induce irreversible attachment in environments with moderate ionic strength (e.g., human body fluids). The increased oxidation degree of GO can introduce more oxygen-containing moieties to enhance electrostatic and hydration repulsion between bacteria and GO.[58,59] Grafting of polymer brushes on GO surface is also a promising alternative to generate strong steric repulsion to prevent bacterial cells from reaching the GO surface.[60,61] Moreover, surface functionalization with antibacterial agents like silver nanoparticles and quaternary ammonium compounds can be employed to prolong the antibiofouling life of GO surfaces by inhibiting biofilm formation.[62]

■ ENVIRONMENTAL IMPLICATION

This work integrates QCM-D, XDLVO theory, and AFM analysis to explore the bacterial attachment to GO surfaces. Our result demonstrates that the bacterial attachment on the GO surface is significantly influenced by ionic strength. The cell densities increase with increasing ionic strength (1−400 mM) and then decrease with a further increase in the ionic strength (600 mM). The weak bacteria−GO interaction at a low ionic strength is mainly driven by electrostatic and steric repulsion, while the low adhesive energy contributes to the reduced bacterial attachment at a high ionic strength. These findings highlight the significance of the ionic strength on bacterial attachment on GO surface, providing a mechanistic understanding of ionic strength-dependent bacteria−GO interactions. Moreover, our results provide an important scientific foundation for the optimization of the antifouling properties of GO in practical applications. Future efforts are needed to characterize other parameters in bacteria−GO interfacial interactions, such as ionic species, pH, presence of dissolved organic matter, and fluid flow shear.

■ ASSOCIATED CONTENT

Supporting Information

The Supporting Information is available free of charge at https://pubs.acs.org/doi/10.1021/acs.est.1c08672.

Full derivation of the quantitative model for QCM-D response; calculation of contact region; XDLVO analysis; density and viscosity of NaCl solutions; surface tension components of *P. aeruginosa* PAO1 and GO; physical properties of biopolymer layer; SEM images of GO; XRD patterns, FTIR spectra, and Raman spectroscopy of GO; cell activity; SEM images of GO-coated sensors; AFM images of GO-coated surface; Raman mapping of QCM-D sensors; biological replicates of QCM-D result; surface cell densities during attachment; equivalent circuit diagram; QCM-D model fitting results; measured and predicted surface cell densities; representative AFM force curve; histograms of F_{peak} and L_R; polymer thickness and grafting density for Δ*pel*-Δ*psl*; interactions energy profiles; and zeta potential of *P. aeruginosa* PAO1 and GO (PDF)

■ AUTHOR INFORMATION

Corresponding Authors

Yichao Wu − *College of Resources and Environment, Huazhong Agricultural University, Wuhan 430070, China; State Key Laboratory of Agricultural Microbiology, Huazhong Agricultural University, Wuhan 430070, China;* orcid.org/0000-0001-7453-6359; Email: wuyichao@mail.hzau.edu.cn

Peng Cai − *College of Resources and Environment, Huazhong Agricultural University, Wuhan 430070, China; State Key Laboratory of Agricultural Microbiology, Huazhong Agricultural University, Wuhan 430070, China;* orcid.org/0000-0002-3103-1542; Email: cp@mail.hzau.edu.cn

Authors

Xinxin Jing − *College of Resources and Environment, Huazhong Agricultural University, Wuhan 430070, China; State Key Laboratory of Agricultural Microbiology, Huazhong Agricultural University, Wuhan 430070, China*

Dengjun Wang − *School of Fisheries, Aquaculture and Aquatic Sciences, Auburn University, Auburn, Alabama 36849, United States;* orcid.org/0000-0002-2047-5260

Chenchen Qu − *College of Resources and Environment, Huazhong Agricultural University, Wuhan 430070, China; State Key Laboratory of Agricultural Microbiology, Huazhong Agricultural University, Wuhan 430070, China*

Jun Liu − *College of Resources and Environment, Huazhong Agricultural University, Wuhan 430070, China; State Key Laboratory of Agricultural Microbiology, Huazhong Agricultural University, Wuhan 430070, China*

Chunhui Gao − *College of Resources and Environment, Huazhong Agricultural University, Wuhan 430070, China; State Key Laboratory of Agricultural Microbiology, Huazhong Agricultural University, Wuhan 430070, China;* orcid.org/0000-0002-1445-7939

https://doi.org/10.1021/acs.est.1c08672
Environ. Sci. Technol. 2022, 56, 16707−16715

Abdelkader Mohamed − *College of Resources and Environment, Huazhong Agricultural University, Wuhan 430070, China; State Key Laboratory of Agricultural Microbiology, Huazhong Agricultural University, Wuhan 430070, China*

Qiaoyun Huang − *College of Resources and Environment, Huazhong Agricultural University, Wuhan 430070, China; State Key Laboratory of Agricultural Microbiology, Huazhong Agricultural University, Wuhan 430070, China;* orcid.org/0000-0002-2733-8066

Noha Mohamed Ashry − *College of Resources and Environment, Huazhong Agricultural University, Wuhan 430070, China; State Key Laboratory of Agricultural Microbiology, Huazhong Agricultural University, Wuhan 430070, China; Agriculture Microbiology Department, Faculty of Agriculture, Benha University, Moshtohor, Qalubia 13736, Egypt*

Complete contact information is available at: https://pubs.acs.org/10.1021/acs.est.1c08672

Notes

The authors declare no competing financial interest.

■ ACKNOWLEDGMENTS

This work was supported by the National Natural Science Foundation of China (42177283, 42177281, and 42225706), the National Key Research and Development Program (2020YFC1806802, 2020YFC1806803), Royal Society Newton Advance Fellowship (NAF/R1/191017), and Fundamental Research Funds for the Central Universities (2662022ZHYJ001).

■ REFERENCES

(1) Wu, Y.; Xia, Y.; Jing, X.; Cai, P.; Igalavithana, A. D.; Tang, C.; Tsang, D. C. W.; Ok, Y. S. Recent advances in mitigating membrane biofouling using carbon-based materials. *J. Hazard. Mater.* **2020**, *382*, No. 120976.

(2) Dong, L.; Yang, J.; Chhowalla, M.; Loh, K. P. Synthesis and reduction of large sized graphene oxide sheets. *Chem. Soc. Rev.* **2017**, *46*, 7306−7316.

(3) Ali, I.; ALOthman, Z. A.; Sanagi, M. M. Green synthesis of iron nano-impregnated adsorbent for fast removal of fluoride from water. *J. Mol. Liq.* **2015**, *211*, 457−465.

(4) Ghaffar, A.; Zhang, L.; Zhu, X.; Chen, B. Porous PVdF/GO nanofibrous membranes for selective separation and recycling of charged organic dyes from water. *Environ. Sci. Technol.* **2018**, *52*, 4265−4274.

(5) Perreault, F.; Jaramillo, H.; Xie, M.; Ude, M.; Nghiem, L. D.; Elimelech, M. Biofouling mitigation in forward osmosis using graphene oxide functionalized thin-film composite membranes. *Environ. Sci. Technol.* **2016**, *50*, 5840−5848.

(6) Zhu, Z.; Jiang, J.; Wang, X.; Huo, X.; Xu, Y.; Li, Q.; Wang, L. Improving the hydrophilic and antifouling properties of polyvinylidene fluoride membrane by incorporation of novel nanohybrid GO@SiO_2 particles. *Chem. Eng. J.* **2017**, *314*, 266−276.

(7) Miao, W.; Li, Z.-K.; Yan, X.; Guo, Y.-J.; Lang, W.-Z. Improved ultrafiltration performance and chlorine resistance of PVDF hollow fiber membranes via doping with sulfonated graphene oxide. *Chem. Eng. J.* **2017**, *317*, 901−912.

(8) Perreault, F.; De Faria, A. F.; Nejati, S.; Elimelech, M. Antimicrobial properties of graphene oxide nanosheets: why size matters. *ACS Nano* **2015**, *9*, 7226−7236.

(9) Chen, J.; Peng, H.; Wang, X.; Shao, F.; Yuan, Z.; Han, H. Graphene oxide exhibits broad-spectrum antimicrobial activity against bacterial phytopathogens and fungal conidia by intertwining and membrane perturbation. *Nanoscale* **2014**, *6*, 1879−1889.

(10) Chen, J.; Wang, X.; Han, H. A new function of graphene oxide emerges: inactivating phytopathogenic bacterium *Xanthomonas oryzae* pv. Oryzae. *J. Nanopart. Res.* **2013**, *15*, No. 1658.

(11) Wuolo-Journey, K.; BinAhmed, S.; Linna, E.; Castrillón, S. R.-V. Do graphene oxide nanostructured coatings mitigate bacterial adhesion? *Environ. Sci-Nano* **2019**, *6*, 2863−2875.

(12) Romero-Vargas Castrillón, S.; Perreault, F.; de Faria, A. F.; Elimelech, M. Interaction of graphene oxide with bacterial cell membranes: Insights from force spectroscopy. *Environ. Sci. Technol. Lett.* **2015**, *2*, 112−117.

(13) Xue, J.; BinAhmed, S.; Wang, Z.; Karp, N. G.; Stottrup, B. L. Romero-Vargas Castrillón, S. Bacterial adhesion to graphene oxide (GO)-functionalized interfaces is determined by hydrophobicity and GO sheet spatial orientation. *Environ. Sci. Technol. Lett.* **2018**, *5*, 14−19.

(14) Rice, D.; Barrios, A. C.; Xiao, Z.; Bogler, A.; Bar-Zeev, E.; Perreault, F. Development of anti-biofouling feed spacers to improve performance of reverse osmosis modules. *Water Res.* **2018**, *145*, 599−607.

(15) Li, Y.; Yuan, H.; von Dem Bussche, A.; Creighton, M.; Hurt, R. H.; Kane, A. B.; Gao, H. Graphene microsheets enter cells through spontaneous membrane penetration at edge asperities and corner sites. *Proc. Natl. Acad. Sci. U.S.A.* **2013**, *110*, 12295−12300.

(16) Chepkwony, N. K.; Berne, C.; Brun, Y. V. Comparative analysis of ionic strength tolerance between freshwater and marine *Caulobacterales* adhesins. *J. Bacteriol.* **2019**, *201*, No. e00061-19.

(17) Ramezanian, S.; Ta, H. X.; Muhunthan, B.; Abu-Lail, N. Role of ionic strength in the retention and initial attachment of *Pseudomonas putida* to quartz sand. *Biointerphases* **2018**, *13*, No. 041005.

(18) Zhao, W.; Walker, S. L.; Huang, Q.; Cai, P. Adhesion of bacterial pathogens to soil colloidal particles: influences of cell type, natural organic matter, and solution chemistry. *Water Res.* **2014**, *53*, 35−46.

(19) Farid, M. U.; Guo, J.; An, A. K. Bacterial inactivation and in situ monitoring of biofilm development on graphene oxide membrane using optical coherence tomography. *J. Membr. Sci.* **2018**, *564*, 22−34.

(20) Alayande, A. B.; Chae, S.; Kim, I. S. Surface morphology-dependent spontaneous bacterial behaviors on graphene oxide membranes. *Sep. Purif. Technol.* **2019**, *226*, 68−74.

(21) Darling, K. E.; Dewar, A.; Evans, T. J. Role of the cystic fibrosis transmembrane conductance regulator in internalization of *Pseudomonas aeruginosa* by polarized respiratory epithelial cells. *Cell. Microbiol.* **2004**, *6*, 521−533.

(22) Høiby, N. Recent advances in the treatment of *Pseudomonas aeruginosa* infections in cystic fibrosis. *BMC Med.* **2011**, *9*, 1−7.

(23) Al Ashhab, A.; Herzberg, M.; Gillor, O. Biofouling of reverse-osmosis membranes during tertiary wastewater desalination: Microbial community composition. *Water Res.* **2014**, *50*, 341−349.

(24) Al Ashhab, A.; Gillor, O.; Herzberg, M. Biofouling of reverse-osmosis membranes under different shear rates during tertiary wastewater desalination: Microbial community composition. *Water Res.* **2014**, *67*, 86−95.

(25) Ismail, S. B.; de La Parra, C. J.; Temmink, H.; van Lier, J. B. Extracellular polymeric substances (EPS) in upflow anaerobic sludge blanket (UASB) reactors operated under high salinity conditions. *Water Res.* **2010**, *44*, 1909−1917.

(26) Frølund, B.; Palmgren, R.; Keiding, K.; Nielsen, P. H. Extraction of extracellular polymers from activated sludge using a cation exchange resin. *Water Res.* **1996**, *30*, 1749−1758.

(27) Meléndrez, D.; Jowitt, T.; Iliut, M.; Verre, A.; Goodwin, S.; Vijayaraghavan, A. Adsorption and binding dynamics of graphene-supported phospholipid membranes using the QCM-D technique. *Nanoscale* **2018**, *10*, 2555−2567.

(28) Torrey, J. D.; Kirschling, T. L.; Greenlee, L. F. Processing and characterization of nanoparticle coatings for quartz crystal microbalance measurements. *J. Res. Natl. Inst. Stand. Technol.* **2015**, *120*, 1−10.

(29) Zou, M.; Wu, Y.; Redmile-Gordon, M.; Wang, D.; Liu, J.; Huang, Q.; Cai, P. Influence of surface coatings on the adhesion of *Shewanella oneidensis* MR-1 to hematite. *J. Colloid. Interface. Sci.* **2022**, *608*, 2955−2963.
(30) Tarnapolsky, A.; Freger, V. Modeling QCM-D response to deposition and attachment of microparticles and living cells. *Anal. Chem.* **2018**, *90*, 13960−13968.
(31) Lambert, R. J.; Mytilinaios, I.; Maitland, L.; Brown, A. M. Monte Carlo simulation of parameter confidence intervals for non-linear regression analysis of biological data using Microsoft Excel. *Comput. Methods Prog. Biomed.* **2012**, *107*, 155−163.
(32) Wu, Y.; Zaiden, N.; Liu, X.; Mukherjee, M.; Cao, B. Responses of exogenous bacteria to soluble extracellular polymeric substances in wastewater: a mechanistic study and implications on bioaugmentation. *Environ. Sci. Technol.* **2020**, *54*, 6919−6928.
(33) Li, X.; Logan, B. E. Analysis of bacterial adhesion using a gradient force analysis method and colloid probe atomic force microscopy. *Langmuir* **2004**, *20*, 8817−8822.
(34) Huang, Q.; Wu, H.; Cai, P.; Fein, J. B.; Chen, W. Atomic force microscopy measurements of bacterial adhesion and biofilm formation onto clay-sized particles. *Sci. Rep.* **2015**, *5*, No. 16857.
(35) Zhang, Y.; Wayner, C. C.; Wu, S.; Liu, X.; Ball, W. P.; Preheim, S. P. Effect of strain-specific biofilm properties on the retention of colloids in saturated porous media under conditions of stormwater biofiltration. *Environ. Sci. Technol.* **2021**, *55*, 2585−2596.
(36) Van Oss, C. J.; Good, R.; Chaudhury, M. Additive and nonadditive surface tension components and the interpretation of contact angles. *Langmuir* **1988**, *4*, 884−891.
(37) Butt, H.-J.; Kappl, M.; Mueller, H.; Raiteri, R.; Meyer, W.; Rühe, J. Steric forces measured with the atomic force microscope at various temperatures. *Langmuir* **1999**, *15*, 2559−2565.
(38) Iyer, S.; Gaikwad, R. M.; Subba-Rao, V.; Woodworth, C. D.; Sokolov, I. Atomic force microscopy detects differences in the surface brush of normal and cancerous cells. *Nat. Nanotechnol.* **2009**, *4*, 389−393.
(39) De Gennes, P. G. Interactions between polymers and surfactants. *J Phys. Chem.* **1990**, *94*, 8407−8413.
(40) Lerner, R. N.; Lu, Q.; Zeng, H.; Liu, Y. The effects of biofilm on the transport of stabilized zerovalent iron nanoparticles in saturated porous media. *Water Res.* **2012**, *46*, 975−985.
(41) Dybwad, G. L. A sensitive new method for the determination of adhesive bonding between a particle and a substrate. *J. Appl. Phys.* **1985**, *58*, 2789−2790.
(42) Pomorska, A.; Shchukin, D.; Hammond, R.; Cooper, M. A.; Grundmeier, G.; Johannsmann, D. Positive frequency shifts observed upon adsorbing micron-sized solid objects to a quartz crystal microbalance from the liquid phase. *Anal. Chem.* **2010**, *82*, 2237−2242.
(43) Jing, X.; Wu, Y.; Shi, L.; Peacock, C. L.; Ashry, N. M.; Gao, C.; Huang, Q.; Cai, P. Outer membrane *c*-type cytochromes OmcA and MtrC play distinct roles in enhancing the attachment of *Shewanella oneidensis* MR-1 cells to goethite. *Appl. Environ. Microbiol.* **2020**, *86*, No. e01941-20.
(44) Xu, Z.; Coriand, L.; Loeffler, R.; Geis-Gerstorfer, J.; Zhou, Y.; Scheideler, L.; Fleischer, M.; Gehring, F. K.; Rupp, F. Saliva-coated titanium biosensor detects specific bacterial adhesion and bactericide caused mass loading upon cell death. *Biosens. Bioelectron.* **2019**, *129*, 198−207.
(45) Tian, K.; Zhang, B.; Ye, S.; Luo, Y. Intermolecular interactions at the interface quantified by surface-sensitive second-order Fermi resonant signals. *J Phys. Chem. C* **2015**, *119*, 16587−16595.
(46) Xu, L.-C.; Vadillo-Rodriguez, V.; Logan, B. E. Residence time, loading force, pH, and ionic strength affect adhesion forces between colloids and biopolymer-coated surfaces. *Langmuir* **2005**, *21*, 7491−7500.
(47) van Loosdrecht, M. C. M.; Norde, W.; Lyklema, J.; Zehnder, A. J. Hydrophobic and electrostatic parameters in bacterial adhesion. *Aquat. Sci.* **1990**, *52*, 103−114.
(48) Shephard, J. J.; Savory, D. M.; Bremer, P. J.; McQuillan, A. J. Salt modulates bacterial hydrophobicity and charge properties influencing adhesion of *Pseudomonas aeruginosa* (PAO1) in aqueous suspensions. *Langmuir* **2010**, *26*, 8659−8665.
(49) Das, T.; Sharma, P. K.; Krom, B. P.; van der Mei, H. C.; Busscher, H. J. Role of eDNA on the adhesion forces between *Streptococcus mutans* and substratum surfaces: influence of ionic strength and substratum hydrophobicity. *Langmuir* **2011**, *27*, 10113−10118.
(50) Chen, G.; Walker, S. L. Fecal indicator bacteria transport and deposition in saturated and unsaturated porous media. *Environ. Sci. Technol.* **2012**, *46*, 8782−8790.
(51) Habimana, O.; Semião, A. J. C.; Casey, E. The role of cell-surface interactions in bacterial initial adhesion and consequent biofilm formation on nanofiltration/reverse osmosis membranes. *J. Membr. Sci.* **2014**, *454*, 82−96.
(52) de Kerchove, A. J.; Elimelech, M. Impact of alginate conditioning film on deposition kinetics of motile and nonmotile *Pseudomonas aeruginosa* strains. *Appl. Environ. Microbiol.* **2007**, *73*, 5227−5234.
(53) Hwang, G.; Kang, S.; El-Din, M. G.; Liu, Y. Impact of an extracellular polymeric substance (EPS) precoating on the initial adhesion of *Burkholderia cepacia* and *Pseudomonas aeruginosa*. *Biofouling* **2012**, *28*, 525−538.
(54) Liu, Y.; Yang, C.-H.; Li, J. Adhesion and retention of a bacterial phytopathogen *Erwinia chrysanthemi* in biofilm-coated porous media. *Environ. Sci. Technol.* **2008**, *42*, 159−165.
(55) van Loosdrecht, M. C.; Lyklema, J.; Norde, W.; Schraa, G.; Zehnder, A. J. The role of bacterial cell wall hydrophobicity in adhesion. *Appl. Environ. Microbiol.* **1987**, *53*, 1893−1897.
(56) Rijnaarts, H. H. M.; Norde, W.; Lyklema, J.; Zehnder, A. J. B. DLVO and steric contributions to bacterial deposition in media of different ionic strengths. *Colloids Surf., B* **1999**, *14*, 179−195.
(57) Abu-Lail, N. I.; Camesano, T. A. Role of ionic strength on the relationship of biopolymer conformation, DLVO contributions, and steric interactions to bioadhesion of *Pseudomonas putida* KT2442. *Biomacromolecules* **2003**, *4*, 1000−1012.
(58) Song, X.; Zambare, R. S.; Qi, S.; Sowrirajalu, B. N. I. L.; James Selvaraj, A. P.; Tang, C. Y.; Gao, C. Charge-gated ion transport through polyelectrolyte intercalated amine reduced graphene oxide membranes. *ACS Appl. Mater. Interfaces* **2017**, *9*, 41482−41495.
(59) Bryjak, M.; Gancarz, I.; Poźniak, G.; Tylus, W. Modification of polysulfone membranes 4. Ammonia plasma treatment. *Eur. Polym. J.* **2002**, *38*, 717−726.
(60) Ma, W.; Chen, T.; Nanni, S.; Yang, L.; Ye, Z.; Rahaman, M. S. Zwitterion-functionalized graphene oxide incorporated polyamide membranes with improved antifouling properties. *Langmuir* **2019**, *35*, 1513−1525.
(61) Ansari, A.; Peña-Bahamonde, J.; Wang, M.; Shaffer, D. L.; Hu, Y.; Rodrigues, D. F. Polyacrylic acid-brushes tethered to graphene oxide membrane coating for scaling and biofouling mitigation on reverse osmosis membranes. *J. Membr. Sci.* **2021**, *630*, No. 119308.
(62) Liu, H.; Liu, X.; Zhao, F.; Liu, Y.; Liu, L.; Wang, L.; Geng, C.; Huang, P. Preparation of a hydrophilic and antibacterial dual function ultrafiltration membrane with quaternized graphene oxide as a modifier. *J. Colloid Interface Sci.* **2020**, *562*, 182−192.

https://doi.org/10.1021/acs.est.1c08672
Environ. Sci. Technol. 2022, 56, 16707−16715